DEEP INELASTIC LEPTON-NUCLEON SCATTERING AT HERA

P. NEWMAN

School of Physics and Astronomy, University of Birmingham, B15 2TT, UK

E-mail: prn@hep.ph.bham.ac.uk

Data from the HERA collider experiments, H1 and ZEUS, have been fundamental to the rapid recent development of our understanding of the partonic composition of the proton and of QCD. This report focuses on inclusive measurements of neutral and charged current cross sections at HERA, using the full available data taken to date. The present precision on the proton parton densities and the further requirements for future measurements at the Tevatron and LHC are explored. Emphasis is also placed on the region of very low Bjorken-x and Q^2. In this region, the 'confinement' transition takes place from partons to hadrons as the relevant degrees of freedom and novel or exotic QCD effects associated with large parton densities are most likely to be observed. Finally, prospects for the second phase of HERA running are discussed.

1 The HERA Collider Experiments

The presence of a point-like probe together with only one initial state hadron makes deep inelastic lepton nucleon scattering (DIS) the ideal environment in which to study the quantum chromodynamics (QCD) of hadronic interactions and to constrain the parton densities of the proton. In the years 1992-2000, the HERA collider experiments, H1 and ZEUS, collected ep data at electron beam energies of 27.5 GeV and proton energies of 820 GeV and 920 GeV, corresponding to ep center-of-mass energies in excess of 300 GeV. The data were split between around 100 pb^{-1} of e^+p collisions and 15 pb^{-1} of e^-p collisions. With the extensions in accessible kinematic phase space afforded by the large center-of-mass energy and the precise electron and hadron reconstruction in the experiments over a wide rapidity range, these data have been used to gain new insights into many aspects of ep collisions.

This article focuses mainly on measurements of inclusive ep cross sections in both neutral current (NC, $ep \to eX$) and charged current (CC, $ep \to \nu X$) reactions throughout the available phase space. In most cases, the full available data from the first phase of HERA running are used. At relatively large momentum transfers, the inclusive cross sections yield important information on the parton densities of the proton. At small momentum transfers, they can be used to search for novel effects in quantum chromodynamics (QCD) associated with the large parton densities observed at the previously unexplored low momentum fractions of the struck quark.

Less inclusive measurements concentrating on other aspects of ep scattering are described elsewhere in these proceedings. The precision QCD tests and studies of the QCD evolution of parton cascades that have been possible through jet measurements are covered by Hirosky.[1] Measurements of the structure of diffractive exchanges and insights into the formation of rapidity gaps in hadronic interactions are discussed by Yamazaki.[2] Searches for new physics at HERA, at the highest $\sqrt{s}$ ever accessed in a collider with an initial state lepton, are covered by Perez.[3]

2 Neutral and Charged Current DIS at Large Q^2

The kinematics of inclusive DIS are usually described by the variables Q^2, the modulus of the squared four-momentum transfer carried by the exchanged electroweak gauge boson, and x, the fraction of the proton's longitudinal momentum carried by the quark that couples to the exchanged boson. Figure 1 illustrates the kinematic regions in which inclusive measurements have been made thus far at HERA.

The NC process takes place via the exchange of virtual photon and Z^0 propagators. The cross section can be expressed in the form

$$\frac{\mathrm{d}\sigma^{\mathrm{NC}}}{\mathrm{d}x\mathrm{d}Q^2} = 2\pi\alpha_{\mathrm{em}}^2 \cdot \left(\frac{1}{Q^2}\right)^2 \cdot \frac{Y_+}{x} \cdot \tilde{\sigma}_{\mathrm{NC}} \ , \qquad (1)$$

where the term α_{em}^2 expresses the dominance of photon exchange over most of the phase space, $1/Q^4$ is the photon propagator term and the reduced cross section $\tilde{\sigma}_{\mathrm{NC}}$ contains helicity factors, weak terms due to Z^0 exchange and structure functions related to the parton densities of the proton. The variables $Y_\pm = 1 \pm (1-y)^2$, dependent on the inelasticity, y, express the helicity dependence of the electroweak

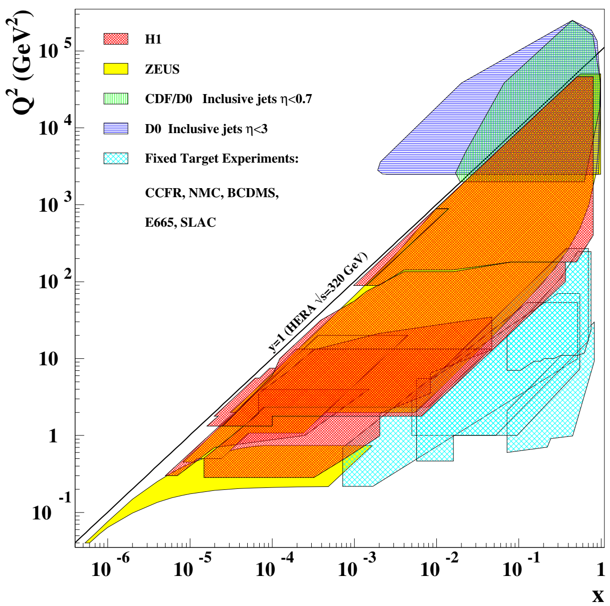

Figure 1. Kinematic plane in x and Q^2 covered by inclusive HERA and fixed-target DIS measurements. The line at inelasticity $y = 1$ represents the kinematic limit. The overlap region with recent jet measurements from the Tevatron[4] is also illustrated.

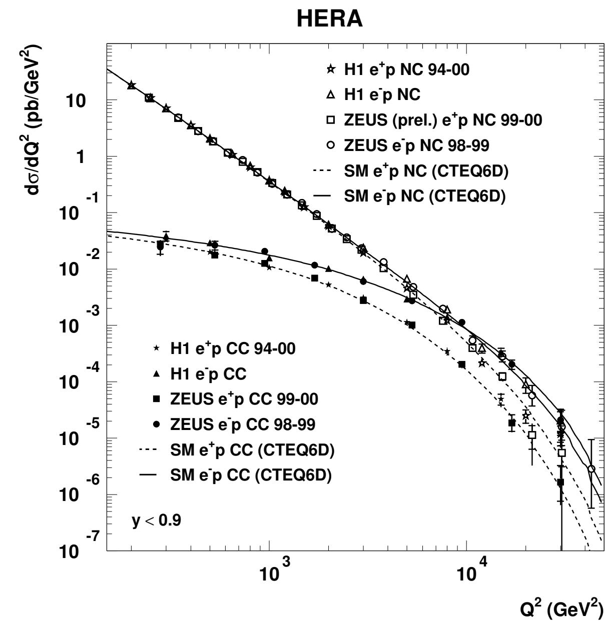

Figure 2. Single differential cross sections for charged and neutral current interactions in $e^{\pm}p$ collisions, as measured by H1 and ZEUS. The data are compared with the predictions of a recent global QCD fit.[11]

interaction (see also Eq. (3)).

The CC process is purely due to weak interactions. The cross section can be expressed as

$$\frac{\mathrm{d}\sigma^{\mathrm{CC}}}{\mathrm{d}x\mathrm{d}Q^2} = \frac{G_F^2 M_W^4}{2\pi} \cdot \left(\frac{1}{Q^2 + M_W^2}\right)^2 \cdot \frac{1}{x} \cdot \tilde{\sigma}_{\mathrm{CC}} \ , \quad (2)$$

where the coupling and propagator terms are specific to W boson exchange and the reduced cross section term $\tilde{\sigma}_{\mathrm{CC}}$ contains the helicity factors and structure functions.

Figure 2 shows the single differential cross sections measured by H1 and ZEUS for charged and neutral current $e^{\pm}p$ scattering with $Q^2 > 200$ GeV^2.[5–10] For $Q^2 \ll M_W^2$, the NC cross section dominates heavily due to the differences between the propagator terms in Eqs. (1) and (2). For $Q^2 \gtrsim M_W^2$, the cross sections for NC and CC processes become comparable, providing an illustration of electroweak unification with space-like gauge bosons. The remaining differences between the NC and CC cross sections in this large Q^2 region and the differences between the e^+p and e^-p cross sections can be understood from the structure of the reduced cross sections $\tilde{\sigma}_{\mathrm{NC}}$ and $\tilde{\sigma}_{\mathrm{CC}}$ (see Secs. 3.2 and 3.3).

At the largest Q^2, the data are sensitive to possible new physics beyond the Standard Model, for example due to quark compositeness. The data have been analyzed in the framework of possible contact interactions,[12] by comparing the measured cross sections with predictions based on parton densities constrained mainly by lower Q^2 and non-HERA data. An example of such a study is shown for NC e^+p interactions in Fig. 3. There is good agreement between the data and the predictions based on the CTEQ5D[13] parton densities up to the highest values of $Q^2 \sim 30\,000$ GeV^2. As a result, quark or electron substructure is excluded down to scales of $\sim 1.0 \times 10^{-18}$ m.

3 Parton Densities

3.1 Current Precision on Parton Densities

Measuring and understanding the parton densities of the proton over as wide a kinematic range as possible is a central aim of HERA analysis. This is important in its own right as a means of improving our understanding of QCD. It is also crucial for precision measurements and the understanding of backgrounds to searches for new physics at the Tevatron and LHC. As can be seen from consideration of the parton kine-

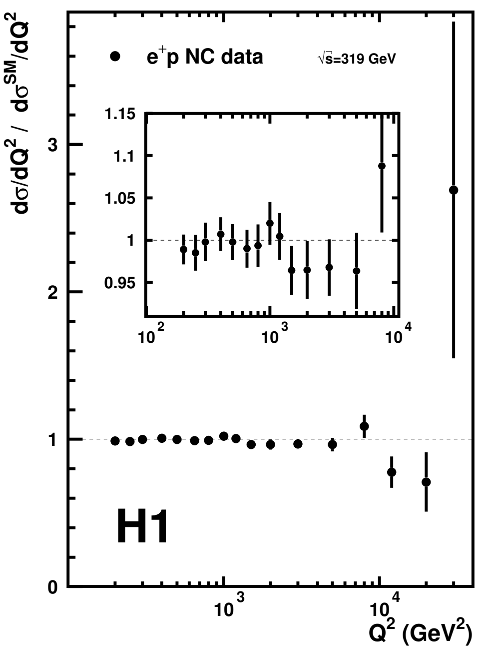

Figure 3. The ratio of H1 data to theoretical prediction for the single differential NC cross section $\mathrm{d}\sigma^{\mathrm{NC}}/\mathrm{d}Q^2$ in e^+p scattering. The theoretical predictions use the CTEQ5D[13] parton densities, which were obtained using only a small fraction of the HERA data.

matics of pp scattering,[14] accurate knowledge of the quark and gluon densities over a wide range of x is necessary to make precise Standard Model calculations for processes such as weak gauge boson, Higgs, or top quark production over the necessary rapidity ranges at these machines.

Figure 4[11] shows estimates of the precision with which the parton densities are currently known. Over the range $10^{-4} \lesssim x \lesssim 10^{-1}$ the combined experimental and theoretical uncertainties on the u and d quark densities are at the level of a few percent,[a] largely thanks to the low x data provided by HERA. The gluon density is somewhat more poorly constrained over this region. At large x values, the uncertainties on all parton densities rapidly increase. This region is crucial for the understanding of backgrounds to the production of any new particles near to threshold in pp scattering. Due to kinematic constraints (Fig. 1), this high x region can only be accessed at HERA at the highest Q^2, where the cross section becomes small (Eq. (1)). Large data samples are therefore needed to improve on the precision obtained from fixed-target or other data in this region. In the following sections, the HERA data used to reach the levels of precision shown in Fig. 4 are presented and discussed in particular in terms of how improvements might be made at large x.

3.2 Neutral Current Cross Sections

The reduced neutral current cross section for $e^{\pm}p$ scattering, corrected for QED-radiative effects, can be expressed as

$$\tilde{\sigma}^{\pm}_{\mathrm{NC}} = F_2 \mp \frac{Y_-}{Y_+}\, xF_3 - \frac{y^2}{Y_+}\, F_L \, , \tag{3}$$

where F_2, xF_3 and F_L are the generalized unpolarized proton structure functions. Extractions of F_2 and xF_3 are described in this section. HERA F_L data are discussed in Sec. 4.3.

The F_2 term is strongly dominant in most of the measured phase space at HERA. After corrections for Z^0 exchange and interference between the photon and Z^0 contributions, the pure electromagnetic structure function F_2^{em} can be extracted. In the quark-parton model, this structure function can be decomposed as

$$F_2^{\mathrm{em}}(x, Q^2) = x \sum_q e_q^2\, (q + \bar{q}) \, , \tag{4}$$

where the sum runs over quark species q of electric charge e_q. F_2^{em} thus provides a squared-charge weighted sum of all quark and antiquark densities. Since $e_u^2 = 4e_d^2$, it yields a particularly strong constraint on the u and $\bar{u}$ contributions.

Figure 5 shows a summary of the F_2^{em} data obtained from e^+p scattering at HERA.[6,10] The structure function is measured over a huge kinematic range and the data are very well described over most of the range by QCD fits (see Sec. (3.4)).[b] The precision reaches $2-3\%$ in the bulk of the phase space. However, in the region of the highest x, the precision of the HERA data remains far from that of fixed-target experiments such as BCDMS[16] and NMC,[17]

[a] This level of precision is only obtained after assumptions are made on the flavor decomposition at low x, which have yet to be tested. For example, all QCD fits assume that $\bar{u} - \bar{d} \to 0$ as $x \to 0$ and assumptions are necessary on the relative contributions from s and c quarks.

[b] A more complete discussion of the various QCD fits performed to DIS and other data and the estimates of the corresponding uncertainties can be found elsewhere in these proceedings.[15]

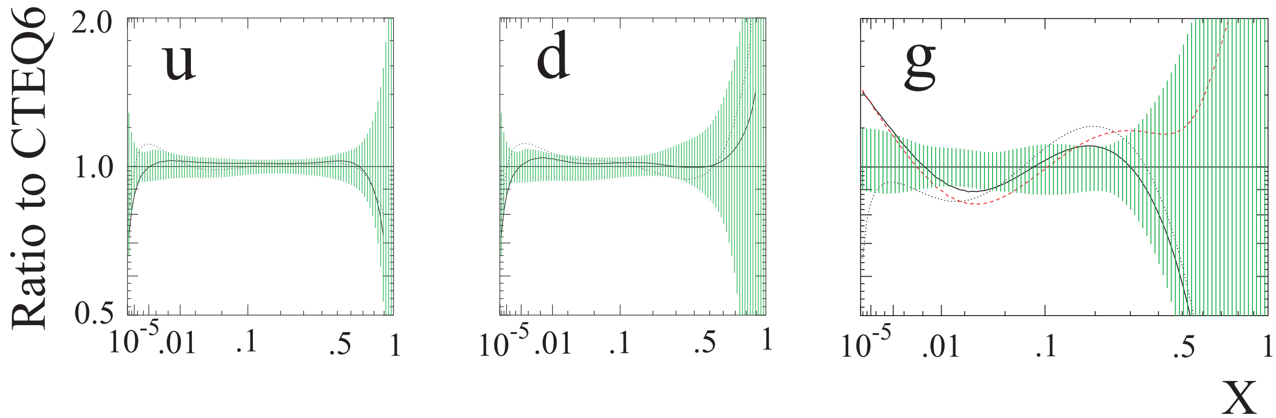

Figure 4. Estimates of the uncertainties on the proton parton densities at $Q^2 = 10$ GeV^2.[11] The bands show the fractional uncertainty as a function of x.

where the smaller center-of-mass energy allows measurements at high x, but lower Q^2. At the highest x, these fixed-target data are not well described by the QCD fits. It is highly desirable to obtain HERA measurements at high x and intermediate Q^2, where the potential problems of the fixed-target data (e.g. higher twist contributions and uncertainties in nuclear corrections) should be absent. This could be achieved with a reasonably large cross section by running HERA with a reduced proton beam energy, as is planned as part of the second phase of HERA running.

The $F_2^{\rm em}$ data also provide the best available constraints on the gluon density via the deviations from Bjorken scaling, caused by gluon radiation. In leading order of QCD, the gluon density can be obtained approximately from $\frac{\partial F_2^{\rm em}(x/2,Q^2)}{\partial \ln Q^2} \sim \alpha_s xg(x)$,[18] such that the strong positive scaling violations at low x in Fig. 5 are indicative of a large and growing gluon density as x becomes small.

The structure function xF_3 arises due to Z^0 exchange. In the HERA phase space, the interference contribution $xF_3^{\gamma Z}$ between the photon and Z^0 exchanges dominates, such that

$$xF_3 = -a_e \, \frac{\kappa Q^2}{Q^2 + M_Z^2} \, xF_3^{\gamma Z} + \Delta(Z^2) \ , \qquad (5)$$

where in the quark-parton model,

$$xF_3^{\gamma Z} = 2x \sum_q e_q a_q (q - \bar{q}) \ . \qquad (6)$$

Here, a_e and a_q are the axial couplings of the Z^0 to electrons and quarks, respectively and $\kappa^{-1} = 4\frac{M_W^2}{M_Z^2}(1 - \frac{M_W^2}{M_Z^2})$ in the on-mass-shell scheme. Since xF_3 measures the difference between the quark and antiquark densities, it is uniquely and model independently sensitive to the non-singlet valence quark densities.

Since it contributes with opposite signs to e^+p and e^-p scattering (Eq. (3)), xF_3 can be extracted from the measured differences between the NC e^+p and e^-p cross sections at large Q^2, shown in Fig. 2, according to

$$xF_3 = \frac{Y_+}{2Y_-} \left(\tilde{\sigma}^-_{\rm NC} - \tilde{\sigma}^+_{\rm NC}\right) \ . \qquad (7)$$

Figure 6 shows the current status of xF_3 data from HERA.[6,8] The data are well described by the predictions of QCD fits in which the valence quark densities are principally constrained by the NC and CC HERA data and measurements from elsewhere, rather than by the differences between the $e^\pm p$ NC cross sections. These measurements thus provide a test of the procedures used and valence densities obtained in QCD fits. The large increases in luminosity expected at HERA-II are required to further exploit this observable.

3.3 Charged Current Cross Sections

In contrast to the NC measurements, where many millions of events are available for analysis, the CC samples collected so far at HERA consist of only around 1500 events (e^+p) and 700 events (e^-p) per experiment. The statistical uncertainties are correspondingly larger than in the NC case, amount-

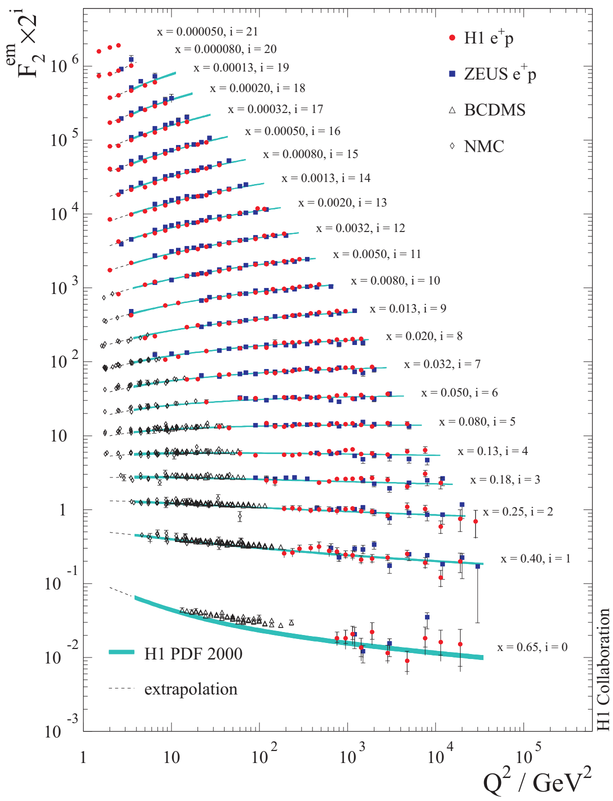

Figure 5. Summary of measurements of the structure function F_2^{em} by H1 and ZEUS. The data are compared with the results of a QCD fit to H1 NC and CC data only.[6]

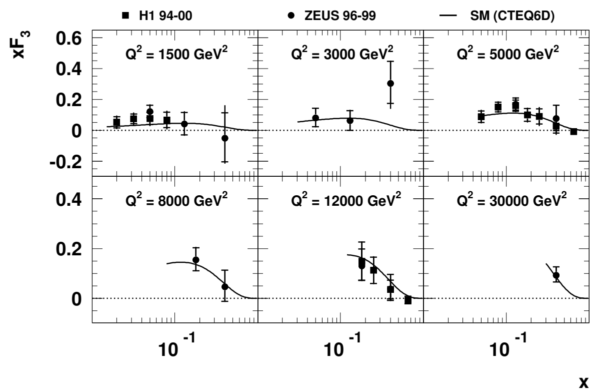

Figure 6. Data on xF_3 from HERA, based on around 100 pb^{-1} of e^+p data and 15 pb^{-1} of e^-p data, compared with the predictions of a recent global fit.[11]

ing to typically 6% for double differential measurements. Charged current cross section measurements do, however, provide important complementary information for the extraction of parton densities, since they are sensitive to particular quark flavors with the correct charges to couple to the exchanged W boson.

As can be seen from Fig. 2, the e^-p CC cross section is significantly larger than the e^+p cross section throughout the measured kinematic range. This is mainly because the e^-p cross section is dominated by the reaction $e^-u \to \nu_e d$, whereas the dominant e^+p process is $e^+d \to \bar{\nu}_e u$, the u density being the larger in the high x region where measurements can be made. In the quark parton model, the charged current reduced cross sections take the form

$$\tilde{\sigma}^-_{\mathrm{CC}} = x(u+c) \;+\; (1-y)^2 \; x(\bar{d}+\bar{s}) \qquad (8)$$

$$\tilde{\sigma}^+_{\mathrm{CC}} = x(\bar{u}+\bar{c}) \;+\; (1-y)^2 \; x(d+s)\;, \qquad (9)$$

where the helicity factor $(1-y)^2$ implies a further kinematic suppression to the term involving the d density in the e^+p case.

The e^-p CC cross section provides a complementary constraint to F_2^{em} on the u density at high x.[5,7] Despite the unfavorable helicity and smaller cross section, the e^-p CC data yield the most direct available constraint on the d density at large x from HERA. This is illustrated in Fig. 7, which shows the most recent measurements from H1[6] and ZEUS.[9] The data are compared with the predictions of a global QCD fit,[11] in which the u and d densities at large x are constrained mainly by precise fixed-target muon scattering data from protons and deuterons. The calculation from the fit is broken down into the contributions from scattering from d-type and $\bar{u}$-type quarks.

The CC measurements should improve considerably with HERA-II data. However, even with 1 fb^{-1}, the uncertainties will remain large in the important region $x \gtrsim 0.5$. An alternative method of constraining the d density at large x would be to run HERA with deuterons[19] and, using isospin symmetry, to unfold the d/u ratio. Running with deuterons at 920 GeV would also naturally reduce the beam energy per nucleon, such that the benefits of the larger cross section at large x and intermediate Q^2 could be exploited.

The ZEUS collaboration[9] have recently used their charged current data to extract a flavor singlet CC structure function,

$$F_2^{\mathrm{CC}} = \frac{2}{Y_+}\left(\tilde{\sigma}^+_{\mathrm{CC}} + \tilde{\sigma}^-_{\mathrm{CC}}\right) + \Delta(xF_3^{\mathrm{CC}}, F_L^{\mathrm{CC}})\;. \qquad (10)$$

This structure function is shown in Fig. 8, where the effects of the small xF_3^{CC} and F_L^{CC} correction

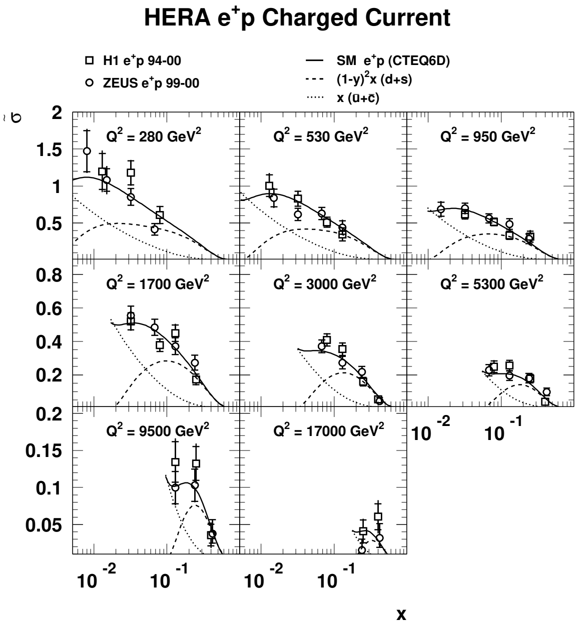

Figure 7. Double differential measurements of the CC e^+p cross section from HERA. The data are compared with the predictions of a recent global fit,[11] which are broken down into contributions from d-type and $\bar{u}$-type quarks.

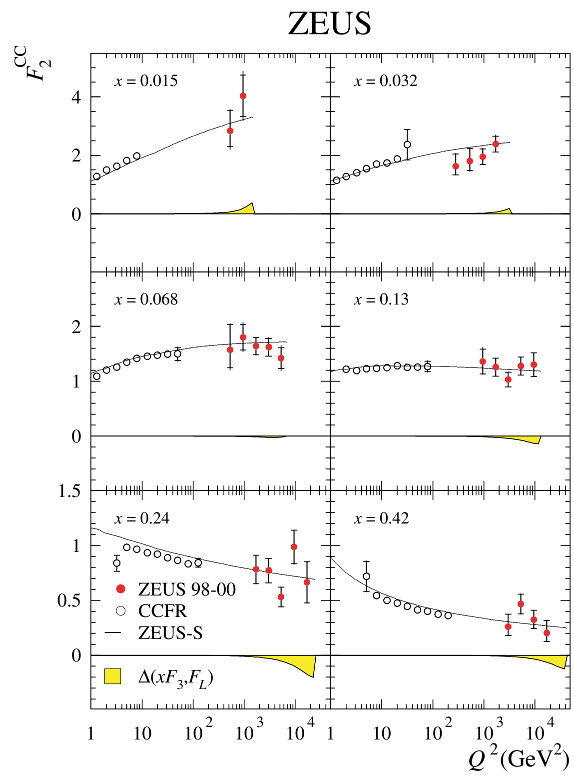

Figure 8. The flavor singlet CC structure function F_2^{CC} as obtained by ZEUS and CCFR. The data are compared with the predictions of a QCD fit to DIS data,[20] which does not include the CC data shown. The corrections necessary for the xF_3^{CC} and F_L^{CC} terms are also illustrated.

terms are also illustrated. The F_2^{CC} results are compared with precise fixed-target neutrino data from CCFR.[21] Viewing the fixed-target and HERA measurements together, the data span more than four orders of magnitude in Q^2 and the influence of gluon radiation on the CC process is clearly visible from the scaling violations. The ZEUS results are well described by the predictions of a QCD fit to various DIS data.[20]

3.4 Parton Density Extractions

The H1[6,22] and ZEUS[20] collaborations, along with various other groups,[11,23,24] have performed QCD fits to extract parton densities using various combinations of HERA and other data. The fits are based on the evolution of the parton densities with Q^2 using the DGLAP equations[25] in Next-to-Leading Order (NLO).[26]

With the latest HERA NC and CC data, it is now possible to extract the full set of flavor-separated parton densities from HERA data alone, provided assumptions are made on the validity of DGLAP evolution throughout the fitted phase space and the quark flavor decomposition at low x. Figure 9 shows the results for the valence densities, the sum of all sea quarks and the gluon density, from H1 NC and CC data only,[6] ZEUS NC data together with other fixed-target DIS experiments,[20] and CTEQ,[11] who perform a global fit to many DIS and other data sets. The agreement between the different extractions is reasonable, though there are differences between the H1 and ZEUS valence densities that go beyond the quoted error bands. This is perhaps not surprising, given the very different sources of information that are used to constrain the valence densities in the two fits. H1 use the limited sensitivity to W and Z exchange effects in the HERA data to separate the valence and sea densities, whereas ZEUS rely mainly on xF_3 data from fixed-target νFe and $\bar{\nu} Fe$ scattering.[27] The shapes of the gluon densities are also rather different. This arises from several sources, including different parameterizations of the parton densities at the starting scale for QCD evolution and

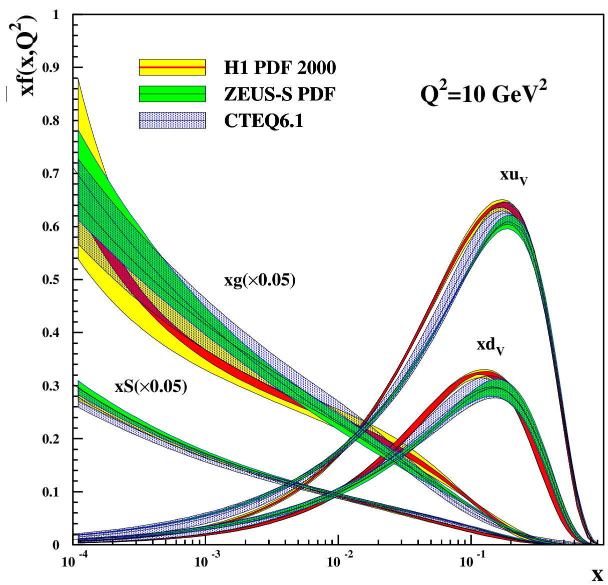

Figure 9. Parton densities as extracted by H1,[6] ZEUS[20] and CTEQ.[11] The sea quark and gluon densities are reduced by a factor of 20 for visibility.

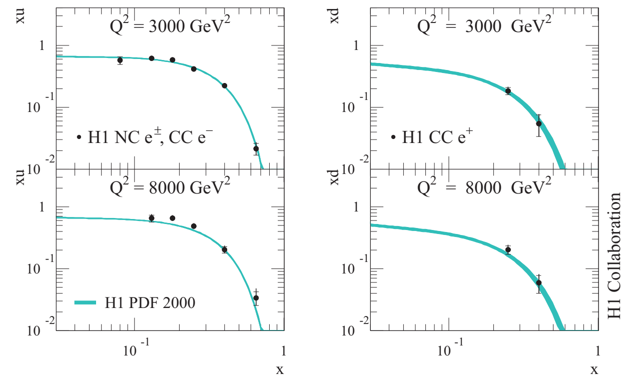

Figure 10. Results from the local extractions of parton densities by H1. The u density is obtained from NC $e^{\pm}$ and CC e^{-} data points for which it contributes in excess of 70% of the cross section. The d density is similarly extracted using CC e^{+} data. The data are compared with the results of a QCD fit to all H1 NC and CC data.[6]

different treatments of heavy quark evolution.[c] As $x \to 1$, the fixed-target data still give the best constraints. Deuteron running at HERA is desirable to test the assumption, used in all fits, that $\bar{d} - \bar{u} \to 0$ as $x \to 0$.[19]

Since the QCD fits rely on various assumptions, it is interesting to extract parton densities directly from the data at fixed values of x and Q^2, in a manner that is relatively insensitive to these assumptions. As shown in Fig. 10, the H1 collaboration has performed such an extraction of the u and d densities at high x using NC and CC data points for which the relevant parton contributes in excess of 70% to the measured cross section according to the H1 QCD fit.[6] The QCD fit is then used to correct for the remaining contributions. The resulting local extractions of the u and d densities are in good agreement with the predictions of the QCD fits using DGLAP evolution.

3.5 Tests of the Gluon Density

The fits to inclusive data rely on the DGLAP QCD evolution equations[25,26] to relate the scaling violations of $F_2^{\rm em}$ to the gluon density and require assumptions on the functional form of the gluon density at the starting scale for QCD evolution. It is important also to constrain the gluon density from other complementary sources with different systematics, in order to test the overall consistency of the HERA data and the validity of the assumptions of DGLAP evolution and QCD hard scattering factorization. This has been done in several ways using hadronic final state data at HERA. Measurements of dijet and charm production cross sections are highly sensitive to the gluon density, since they proceed dominantly via the boson-gluon fusion process $\gamma^* g \to q\bar{q}$, the cross section for which is directly proportional to the gluon density at leading order of QCD. The gluon density can thus be extracted in a manner which is more sensitive to local variations.

Examples of jet data that are sensitive to the gluon density are given by Hirosky.[1] An example of recent charm data that constrain the gluon density can be found in Fig. 11, which shows the cross section for D^* production in DIS as a function of pseudorapidity, as measured by the ZEUS collaboration.[30] The data are compared with a theoretical prediction[31] based on NLO QCD matrix elements, interfaced to the gluon density from a fit to inclusive DIS measurements[20] and to fragmentation functions. The beautiful agreement of the data and theory confirms the gluon density from scaling violations and the validity of the NLO DGLAP theory at the 10% level. The theoretical errors, dominated by the choice of the charm quark mass m_c, are larger than the uncertainties on the data. Comparing the predictions using the ZEUS and CTEQ[13] parton densities shows that the data can be used to

[c]The gluon densities are thus defined in different schemes and strictly speaking cannot be compared directly.

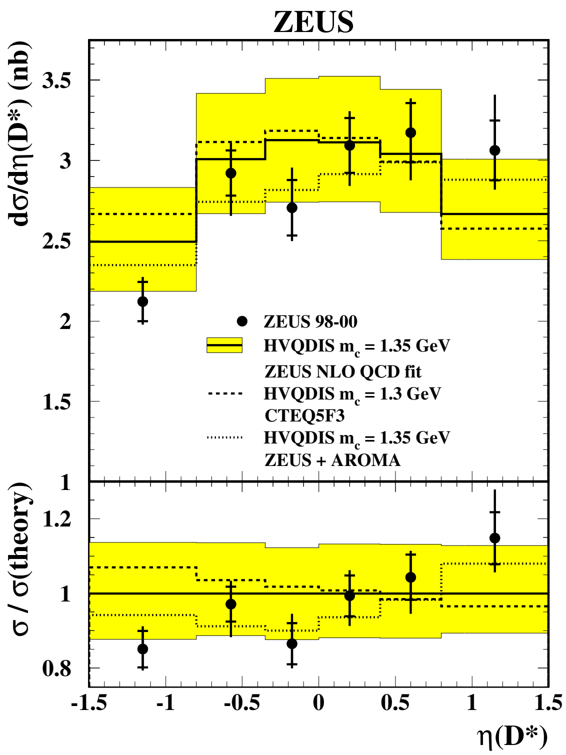

Figure 11. Cross section for D^* meson production in DIS, differential in pseudorapidity. The data are compared with the predictions of a NLO QCD calculation based on parton densities from a fit to DIS data,[20] together with an estimate of the theoretical uncertainties. The effects of switching to the CTEQ5F3 parton densities[13] or to Lund[28] rather than Petersen[29] fragmentation (ZEUS + AROMA) are also indicated.

improve the constraints on the gluon density once the theoretical errors are better controlled.

By extrapolating the D^* cross sections in the measured range of pseudorapidity and transverse momentum to a charm production cross section integrated over the full phase space, it is possible to extract $F_2^{c\bar{c}}$, the charm contribution to the proton structure function F_2.[30,32] For $Q^2 \gg m_c^2$, such that the charm mass can be neglected, the ratio $F_2^{c\bar{c}}/F_2$ becomes close to 30% at low x, illustrating the importance of a proper treatment of the evolution of heavy quarks in any fit to HERA data.

4 The Low x Region

4.1 Low x Physics

The region of low x, newly accessed at HERA, has been the subject of much debate. The fast rise of the gluon density (Fig. 9) raises the question of whether unitarization effects may become important.[d] As the gluon density becomes large, the partons must ultimately begin to interact through processes such as gluon recombination ($gg \to g$).[34] This would lead to a taming of the low x rise of F_2 and a breakdown of the DGLAP approximation.

A full perturbative QCD expansion gives rise to evolution of parton densities with both $\ln Q^2$ and $\ln 1/x$. Standard DGLAP evolution is equivalent to a resummation of leading $\ln Q^2$ terms, such that the struck quark originates from a parton cascade ordered in virtuality. At sufficiently low x, evolution in $\ln 1/x$ must also become important, though it is not incorporated in the DGLAP approximation. Other approximations to QCD evolution may then become more appropriate. Examples are BFKL evolution,[35] which resums the $\ln 1/x$ terms to all orders, or CCFM evolution,[36] in which the partons are ordered in the angle at which they are emitted. CCFM evolution is equivalent to BFKL evolution for $x \to 0$, whilst limiting to the DGLAP equations at larger x.

It has been suggested that the inclusion of BFKL effects improves the description of low x inclusive measurements by QCD fits,[37] though no clear consensus exists on this question. There are also hints from various hadronic final state analyses that regions of phase space can be found at HERA for which standard DGLAP evolution is insufficient and CCFM evolution may provide a better description.[38]

Due to kinematic correlations (Fig. 1), low x values can only be accessed at low Q^2. The low Q^2 regime brings its own complications, such as possible higher twist contributions and the breakdown of convergence of perturbative QCD as the strong coupling increases. Around $Q^2 = 1$ GeV^2, the "confinement" transition takes place, such that the partons of asymptotic freedom are replaced by hadrons as the relevant degrees of freedom.

4.2 F_2 at Low Q^2

The data used in the measurements and QCD fits described in Sec. 2 cover the range $Q^2 \gtrsim 3$ GeV^2, where perturbative QCD can reliably be used. The ZEUS

[d] It has been argued that the conventional Froissart unitarity bound on hadronic total cross sections is not applicable to off-shell virtual photons.[33]

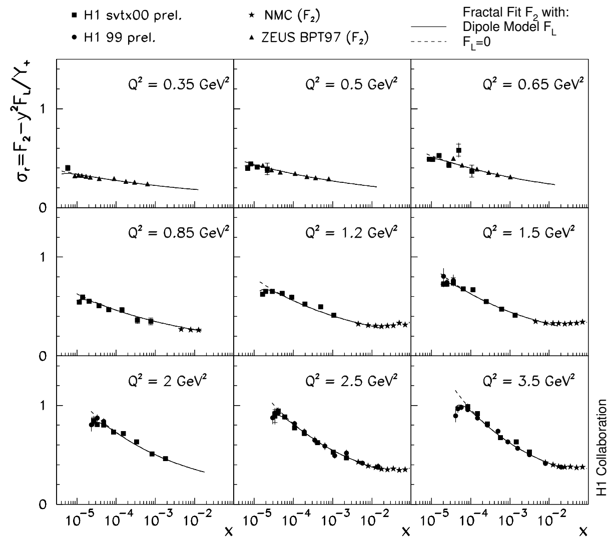

Figure 12. The reduced neutral current cross section $\tilde{\sigma}_{\rm NC}$ at low Q^2. The data are compared with the predictions of a 'fractal' model of proton structure.[41]

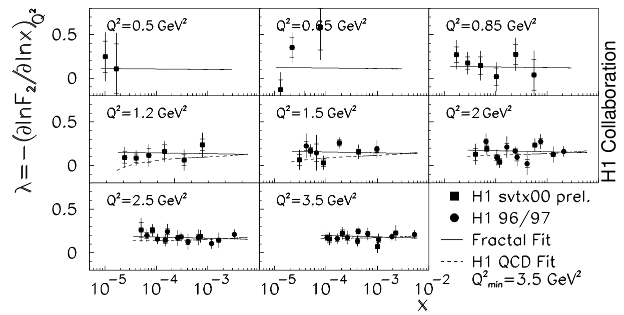

Figure 13. The logarithmic x derivative of F_2 in the low Q^2 region. The data are compared with the predictions of a 'fractal' model of proton structure.[41]

collaboration has obtained precise data (BPT97) in the range $0.0045 < Q^2 < 0.65$ GeV^2, using a silicon strip tracking detector and an electromagnetic calorimeter very close to the beampipe.[39] Previously, the intermediate region, $0.65 < Q^2 \lesssim 3$ GeV^2 has been only poorly explored at HERA, due to the acceptance limitations of the main detectors at small electron scattering angles. In order to improve this acceptance, a short run was taken in the year 2000 with the ep vertex shifted by 70 cm in the outgoing proton direction. The H1 collaboration has recently reported new inclusive NC measurements in the region $0.35 < Q^2 < 3.5$ GeV^2, using these data.[40] The resulting inclusive cross section measurements are shown in the form of the reduced cross section $\tilde{\sigma}_{\rm NC}$ in Fig. 12. The new data span the transition from a fast rise of the cross section with decreasing x at $Q^2 = 3.5$ GeV^2 to a soft rise, similar to that observed in the energy dependence of hadron-hadron total cross sections,[42] at $Q^2 = 0.35$ GeV^2. At the lowest x values, a decrease in the cross section is observed due to the F_L term in Eq. (3) (see also Sec. 4.3).

In the double asymptotic limit,[43] the DGLAP equations can be solved with a solution whereby F_2 rises approximately as a power of x as x becomes small, such that $F_2 \sim x^{-\lambda}$. This feature is also predicted from the BFKL equations. Since unitarization effects would be expected to tame this growth, extracting λ has been suggested[44] as a means of searching for saturation effects. λ corresponds to the logarithmic x derivative of F_2 at fixed Q^2,

$$\lambda(x, Q^2) = (\partial \ln F_2 / \partial \ln x)_{Q^2} \ , \tag{11}$$

which has been extracted locally from the differences between neighboring data points in x by the H1 collaboration.[40,45] The results in the kinematic region of the shifted vertex data are shown in Fig. 13. The data here and at larger Q^2 are consistent with no dependence of λ on x for fixed Q^2 and $x \lesssim 10^{-2}$, and thus with a monotonic rise of F_2 as x decreases with Q^2 fixed. There is thus no evidence for any taming of this rise in inclusive electroproduction data from HERA.

Since the logarithmic x derivative is compatible with independence of Q^2, the proton structure function at low x can indeed be parameterized as

$$F_2 = c(Q^2) \cdot x^{-\lambda(Q^2)} \ . \tag{12}$$

H1 and ZEUS have both fitted their data to this form.[40,45,46] The results for $\lambda(Q^2)$ are shown in Fig. 14. Two distinct regions seem to be distinguished. For $Q^2 \gtrsim 3$ GeV^2, where partons are the relevant degrees of freedom, λ depends logarithmically on Q^2 and $c \sim 0.18$ is consistent with being constant. This behavior is well reproduced by DGLAP-based QCD fits. In contrast, for $Q^2 \lesssim 1$ GeV^2, there is evidence for a decrease in $c(Q^2)$ and for deviations of $\lambda(Q^2)$ from the logarithmic dependence on Q^2 as it tends to the value of 0.08 known to describe hadron-hadron[42] and photoproduction[47] total cross sections. In this region, the description by DGLAP breaks down as the confinement transition takes place on a distance scale of around 0.3 fm.

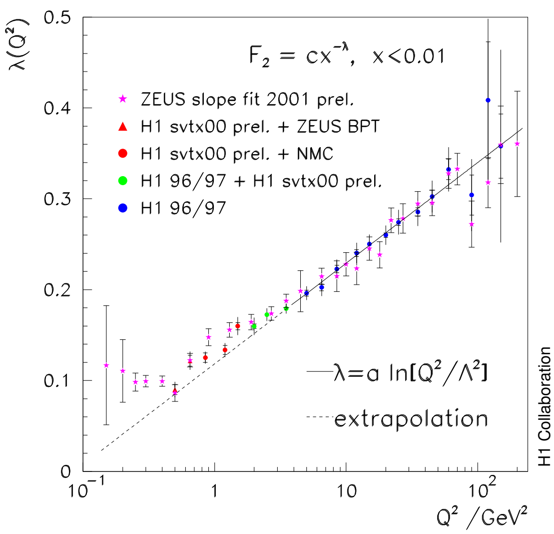

Figure 14. The results for λ from fits to low x data of the form $F_2 \sim x^{-\lambda}$. The data are compared with a parameterization in which λ grows logarithmically with Q^2.

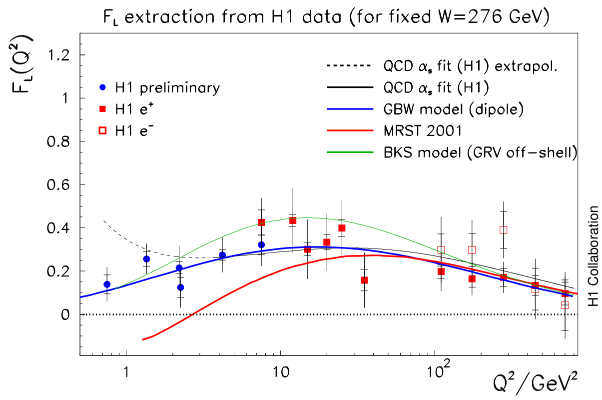

Figure 15. Summary of H1 F_L determinations shown at fixed photon-proton center-of-mass energy $W = 276$ GeV. The data are compared with the predictions of a QCD fit to H1 NC and CC data only,[6] a global QCD fit,[23] a phenomenological dipole model[50] and a model based on unintegrated parton densities and k_T factorization.[51].

4.3 F_L at Low Q^2

As can be seen from Fig. 12, the effects of F_L are visible in the inclusive reduced cross section at the lowest x, or highest y values. In this region, the scattered electron energy becomes very small and background from processes at $Q^2 \simeq 0$ in which a hadron is misidentified as the scattered electron becomes large. The H1 collaboration is able to make measurements for scattered electron energies as low as 3 GeV with the help of drift chambers and a silicon tracking detector accompanying the backward calorimeter. These detectors allow the event vertex to be reconstructed from the electron track at high y and enable the suppression of photoproduction background by ensuring that a track of the correct charge is linked to the electron candidate calorimeter cluster.

F_L is identically zero in lowest order QCD, but acquires a non-zero value at $\mathcal{O}(\alpha_s)$ due to gluon radiation. It is thus able to play a similar role to dijet and charm data (Sec. 3.5) in providing complementary information on the gluon density to that obtained from the scaling violations of F_2 assuming DGLAP evolution. This is particularly important at low x, where the Q^2 range of HERA F_2 measurements is rather small (see Fig. 1), dijet and charm measurements cannot be made due to kinematic restrictions and DGLAP evolution is most questionable. The sensitivity to F_L at high y, visible in Fig. 12, has been exploited to determine F_L in the crucial region around $Q^2 = 1$ GeV^2.

The determination is made by fitting the reduced cross section to the form

$$\tilde{\sigma}_{\rm NC} = F_2 - (y^2/Y_+)\ F_L \qquad (13)$$
$$= c(Q^2) \cdot x^{-\lambda(Q^2)} - (y^2/Y_+)\ F_L\ , \qquad (14)$$

where the second equality follows from Eq. (12) and at each Q^2 value, c, λ and F_L are free parameters. The results of the extraction are insensitive to the assumptions on the behavior of F_2 at the present level of accuracy. The shape of the low x turn-over of $\tilde{\sigma}_{\rm NC}$ is driven by the y^2/Y_+ dependence, such that F_L can only be extracted at a single point in x. The results are shown as a function of Q^2 in Fig. 15, together with other F_L extractions using similar methods, spanning three orders of magnitude in Q^2.[5,6,48,49] The data are compared with a variety of predictions based on DGLAP QCD fits[22,23] and other phenomenological approaches.[50,51] The data show that F_L remains non-zero down to the lowest Q^2 values measured and already distinguish between the different models in the low x region.

Significant further progress in F_L measurements at HERA can only be made by reducing the proton beam energy, such that the F_2 and F_L terms in Eq. (13) can be separated through measurements at the same x and Q^2, but different y. This would remove the need for assumptions on the behavior of F_2

in the region where F_L effects are present and would allow measurements of the x dependence, providing further important discrimination between models.

5 Future Prospects

The HERA accelerator has recently restarted providing collisions, following a shutdown during which it was upgraded to provide a factor of around four increase in instantaneous luminosity. Spin rotators and polarimeters have also been placed around the electron ring, so that the effects of longitudinal polarisation of the electrons can be studied. In parallel, many upgrades have been made to the H1 and ZEUS detectors, including improved silicon tracking, forward tracking and track-based triggering. These improvements should improve the quality of data on charmed hadrons in particular and should extend the accessible phase space for many final state measurements towards higher x.

Over the next few years, the aim is to collect 1 fb^{-1} of data, representing a factor of 10 increase in statistics, equally shared between positron and electron running with positive and negative lepton helicities. A run with reduced proton beam energies in order to measure F_L and access the high x, intermediate Q^2 region is also planned. Further options for the running of HERA, for example replacing the proton beam with deuterons or heavier ions or polarising the proton beam in order to study nucleon spin at low x, do not currently form part of the future plans.

6 Summary

The data from the first phase of HERA running have now been fully analyzed from the point of view of high Q^2 inclusive charged and neutral current cross sections. The resulting data provide the best available constraints on the proton quark and gluon densities in the region $10^{-4} < x < 10^{-1}$, crucial for future experimentation at the Tevatron and LHC. Further improvements at larger x are possible in the future with higher luminosities and reduced proton energy running. The data on hadronic final states are highly sensitive to the QCD of hadronic interactions and complement the inclusive measurements, providing tests of the QCD evolution equations and competitive information on the gluon density. Here, improvements in the precision of theoretical calculations are required in order to make significant further progress. There have been considerable recent developments in understanding the region of low x and Q^2 and testing the range of validity of DGLAP evolution. With the HERA-II run just beginning, the prospects are exciting for future measurements.

Acknowledgments

I would like to acknowledge the work of all members of the H1 and ZEUS collaborations, which has led to the many impressive results shown in this article. I would also like to thank J. Butterworth, V. Chekelian, E. Elsen, T. Greenshaw, B. Heinemann, V. Hudgson, M. Klein, T. Laštovička, K. McFarland, D. Naples, E. Rizvi, R. Thorne and R. Wallny for help with the preparation of this presentation and/or for proof-reading this manuscript.

References

1. R. Hirosky, these proceedings.
2. Y. Yamazaki, these proceedings.
3. E. Perez, these proceedings.
4. D0 Collaboration, *Phys. Rev. Lett.* **82**, 2451 (2001); CDF Collaboration, *Phys. Rev.* D **64**, 032001 (2001).
5. H1 Collaboration, *Eur. Phys. J.* C **19**, 269 (2001).
6. H1 Collaboration, *Eur. Phys. J.* C **30**, 1 (2003).
7. ZEUS Collaboration, *Phys. Lett.* B **539**, 197 (2002).
8. ZEUS Collaboration, *Eur. Phys. J.* C **C28**, 175 (2003).
9. ZEUS Collaboration, DESY 03-093, submitted to *Eur. Phys. J. C.*
10. ZEUS Collaboration, paper 630 submitted to International Europhysics Conference on High Energy Physics (EPS01), Budapest, Hungary, July 2001.
11. J. Pumplin *et al.*, *JHEP* **0207**, 012 (2002).
12. H1 Collaboration, *Phys. Lett.* B **568**, 35 (2003); ZEUS Collaboration, *Eur. Phys. J.* C **14**, 239 (2000).
13. H. Lai *et al.*, *Eur. Phys. J.* C **12**, 375 (2000).
14. A. Martin *et al.*, *Eur. Phys. J.* C **14**, 133 (2000).
15. R. Thorne, these proceedings.
16. BCDMS Collaboration, *Phys. Lett.* B **223**, 485 (1989).
17. NMC Collaboration, *Phys. Lett.* B **364**, 107 (1995).
18. K. Prytz, *Phys. Lett.* B **311**, 286 (1993).
19. T. Alexopoulos *et al.*, *"Electron-Deuteron Scattering at HERA, a Letter of Intent for an Experimental Programme with the H1 Detector"*, DESY-PRC 03/02 (available from http://www-h1.desy.de/h1/www/publications/H1eDLoI.pdf).
20. ZEUS Collaboration, *Phys. Rev.* D **67**, 012007 (2003).

21. CCFR/NuTeV Collaboration, *Phys. Rev. Lett.* **86**, 2742 (2001).
22. H1 Collaboration, *Eur. Phys. J.* C **21**, 33 (2001).
23. A. Martin *et al.*, *Eur. Phys. J.* C **23**, 73 (2002).
24. S. Alhekin, *Phys. Rev.* D **68**, 114002 (2003).
25. V. Gribov and L. Lipatov, *Sov. J. Nucl. Phys.* **15**, 438 & 675 (1972);
    L. Lipatov, *Sov. J. Nucl. Phys.* **20**, 94 (1975);
    G. Altarelli and G. Parisi, *Nucl. Phys.* B **126**, 298 (1977);
    Y. Dokshitzer, *Sov. Phys. JETP* **46**, 641 (1977).
26. W. Furmanski and R. Petronzio, *Phys. Lett.* B **97**, 437 (1980).
27. CCFR Collaboration, *Phys. Rev. Lett.* **79**, 1213 (1997).
28. B. Andersson *et al.*, *Phys. Rep.* **97**, 31 (1983).
29. C. Petersen *et al.*, *Phys. Rev.* D **27**, 105 (1983).
30. ZEUS Collaboration, DESY-03-115, submitted to *Phys. Rev.* D.
31. B. Harris and J. Smith, *Phys. Rev.* D **57**, 2806 (1998).
32. H1 Collaboration, *Phys. Lett.* B **528**, 199 (2002).
33. S. Troshin and N. Tyurin, *Eur. Phys. J.* C **22**, 667 (2002).
34. L. Gribov, E. Levin and, M. Ryskin, *Nucl. Phys.* B **188**, 555 (1981);
    L. Gribov, E. Levin and M. Ryskin, *Phys. Rep.* **100**, 1 (1983).
35. V. Fadin, E. Kuraev and L. Lipatov, *Sov. Phys. JETP* **44**, 443 (1976);
    V. Fadin, E. Kuraev and L. Lipatov, *Sov. Phys. JETP* **45**, 199 (1977);
    Y. Balistsky and L. Lipatov, *Sov. J. Nucl. Phys.* **28**, 822 (1978).
36. M. Ciafaloni, *Nucl. Phys.* B **296**, 49 (1988);
    S. Catani, F. Fioriani and M. Marchesini, *Phys. Lett.* B **234**, 339 (1990);
    S. Catani, F. Fioriani and M. Marchesini, *Nucl. Phys.* B **336**, 18 (1990);
    M. Marchesini, *Nucl. Phys.* B **445**, 49 (1995).
37. R. Thorne, *Phys. Rev.* D **60**, 054031 (1999).
38. H1 Collaboration, *Nucl. Phys.* B **538**, 3 (1999);
    ZEUS Collaboration, *Eur. Phys. J.* C **6**, 239 (1999);
    ZEUS Collaboration, *Phys. Lett.* B **474**, 223 (2000);
    H1 Collaboration, *Phys. Lett.* B **542**, 193 (2002).
39. ZEUS Collaboration, *Phys. Lett.* B **487**, 53 (2000).
40. H1 Collaboration, paper 975 submitted to International Conference on High Energy Physics (ICHEP02), Amsterdam, Holland, July 2002.
41. T. Laštovička, *Eur. Phys. J.* C **24**, 529 (2002).
42. A. Donnachie and P. Landshoff, *Phys. Lett.* B **296**, 227 (1992).
43. A. De Rujula *et al.*, *Phys. Rev.* D **10**, 1649 (1974);
    R. Ball and S. Forte, *Phys. Lett.* B **335**, 77 (1994).
44. H. Navelet, R. Peschanski and S. Wallon, *Mod. Phys. Lett.* A **9**, 3393 (1994).
45. H1 Collaboration, *Phys. Lett.* B **520**, 183 (2001).
46. ZEUS Collaboration, *Eur. Phys. J.* C **7**, 609 (1999).
47. H1 Collaboration, *Zeit. Phys.* C **69**, 27 (1995);
    ZEUS Collaboration, *Nucl. Phys.* B **627**, 3 (2002).
48. H1 Collaboration, paper 83 submitted to International Europhysics Conference on High Energy Physics (EPS03), Aachen, Germany, July 2003.
49. H1 Collaboration, paper 799 submitted to International Europhysics Conference on High Energy Physics (EPS01), Budapest, Hungary, July 2001.
50. K. Golec-Biernat and M. Wüsthoff, *Phys. Rev.* D **59**, 014017 (1999).
51. B. Badelek, J. Kwieciński and A. Staśto, *Zeit. Phys.* C **74**, 297 (1997).

DISCUSSION

Thomas Gehrmann (Zürich University): Concerning the measurement of $F_2^{c\bar{c}}$, you mention that you obtain $F_2^{c\bar{c}}$ from an extrapolation of the charmed hadron spectra. Could you please comment on how much $F_2^{c\bar{c}}$ is actually measurement, and how much is extrapolation? And: how big is the error due to the extrapolation?

Paul Newman: The extrapolations can be large. For the ZEUS measurement shown, they vary from a factor of 5 at low Q^2 to a factor of 1.5 at high Q^2. They are done using NLO QCD programs, the uncertainties are assessed and included in the quoted errors. They are not the dominant uncertainties, though assessing the full extrapolation errors is non-trivial.

Rik Yoshida (ZEUS spokesman, Argonne, paraphrased by PN): While the systematic errors for the extrapolation of the D^* cross section to $F_2^{c\bar{c}}$ are evaluated, the extraction of $F_2^{c\bar{c}}$ is necessarily a model dependent procedure. It is better to compare models of charm production with the data directly at the level of the measured differential cross sections. It is difficult to assess the correctness of models that only predict $F_2^{c\bar{c}}$ or the total charm cross section.

Paul Newman: That is a very good point. The usefulness of $F_2^{c\bar{c}}$ lies mainly in the illustration of the charm contribution to F_2 as a function of the more familiar variables x and Q^2.

Ikaros Bigi (University of Notre Dame du Lac): Do you see any evidence for intrinsic charm in the data, or what is the status of this ancient concept?

Paul Newman (paraphrased and extended): Our data are consistent with the charm component being entirely due to QCD evolution and thus related to the gluon density. With the present data, there is no need for an additional source. However, better data in the high x region where intrinsic charm contributions have previously been discussed are likely to become available at HERA-II, now that charm triggers and forward tracking have been improved.